Title
Beyond the Pre-Equilibrium Approximation: Consequences of Elementary Step (Ir)reversibility on the Mechanistic Interpretation of Tafel Slope

Journal
Angewandte Chemie International Edition, 65(25)

ISSN
1433-7851

Author
Razdan, Neil K

Publication Date
2026-06-15

DOI
10.1002/anie.1052729

SCIENTIFIC PERSPECTIVE

Beyond the Pre-Equilibrium Approximation: Consequences of Elementary Step (Ir)reversibility on the Mechanistic Interpretation of Tafel Slope

Neil K. Razdan*[a]

[a] Prof. N. K. Razdan
Department of Chemical and Biomolecular Engineering
University of California Berkeley
Berkeley, CA, 94720
E-mail: razdan@berkeley.edu

Supporting information for this article is given via a link at the end of the document.

Biographical sketch. Neil K. Razdan received his BS (2017) and PhD (2022) in Chemical Engineering at UC Berkeley and the University of Minnesota respectively. He was as an Arnold O. Beckman Postdoctoral Fellow at MIT where he developed analytical methods and conceptual advances to bridge thermochemical and electrochemical catalysis. In July 2024, he joined UC Berkeley as an Assistant Professor in the Department of Chemical and Biomolecular Engineering. He leads a research group focused on kinetic and mechanistic characterization of catalysts for (electro)chemical energy conversion.

Abstract: The relationship between electrochemical potential and reaction rate—or Tafel slope—is fundamental to the study of multi-step charge transfer reactions. However, despite its importance and ubiquitous use, Tafel slope is seldom interpreted outside of 'cardinal' values. The mechanistic interpretation of cardinal Tafel slopes is predicated on the pre-equilibrium approximation (PEA): that the path between the (catalyst) resting state and rate-determining step is in equilibrium. This stringent approximation severely limits opportunities to elicit mechanistic information from electrochemical processes. In this Scientific Perspective, we broaden the existing framework for mechanistic interpretation of Tafel slope through a simple, universal equation that generally describes Tafel slope in terms of elementary-step symmetry factors and approach-to-equilibrium (i.e., approach to PEA accuracy). The predictiveness and mechanistic utility of these theoretical developments is showcased through analysis of experimental data available in the literature for a broad range of electrochemical and thermochemical catalytic reactions including O_2, H_2, Cl_2, and CO redox. The learnings accrued in these case studies inform kinetic study of all multi-step charge transfer reactions and are particularly relevant for mixed-potential-driven mechanisms of thermochemical catalysis, which in recent years have been shown to be preponderant at metal-liquid interfaces.

1. Introduction

Multi-step charge transfer reactions comprise a tremendous range of natural and synthetic processes including biological redox, interfacial ion transfer, corrosion, and molecular and heterogeneous (electro)catalysis. In each of these cases, the relationship between electrochemical potential (E) and reaction rate, or current, is fundamental to developing a mechanistic understanding of charge transfer[1–5]. The E-dependence of the reaction rate (r) is conventionally formulated in terms of either the Tafel slope

$$b \equiv \frac{\partial E}{\partial \log_{10} r} \quad \textbf{(1)}$$

or the transfer coefficient, a dimensionless alternative defined as

$$\alpha \equiv \frac{RT}{F}\frac{\partial \ln r}{\partial E} = \ln 10 \frac{RT}{F} \times {}^{1}/_{b} \quad \textbf{(2)}$$

where R is the gas constant, T is temperature, and F is the Faraday constant. Measurement of Tafel slope (b) or transfer coefficient (α) is typically straightforward. However, in contrast to its ease of measurement, the *interpretation* of Tafel slope in terms of the kinetics and thermodynamics of constituent molecular charge-transfer events is far more challenging. Even for individual elementary steps, the relationship between reaction rate and electrochemical potential is complicated by an expansive diversity in extents of charge-transfer adiabaticity, coupling of nuclear and electronic motion, and requirements for solvent reorganization[6–10]. This complexity is further exacerbated in multi-step reactions in which each microscopic charge-transfer step contributes to the observed, macroscopic rate–potential relationship (Tafel slope) in a generally uncertain fashion. These challenges have so far prevented formulation of a general equation for Tafel slope in terms of elementary-step kinetics and thermodynamics. Instead, mechanistic interpretation of Tafel slope has historically relied on invocation of a set of limiting assumptions that appear to explain common observation of 'cardinal', or near half-integer, transfer coefficients ($\alpha \approx$ ½, 1, 1 ½, 2). Stated mathematically, 'cardinal' transfer coefficients are described by **Eq. 3:**

$$\alpha = \beta_{RDS} n_{RDS} + \frac{n_{pre-RDS}}{\sigma_{RDS}} \quad \textbf{(3)}$$

where the subscript RDS refers to the rate-determining step; β_{RDS}, σ_{RDS}, and n_{RDS} are respectively the symmetry factor of, stoichiometric number of, and the number of electrons transferred in the RDS; and, $n_{pre-RDS}$ is the number of electrons transferred 'before' the RDS—meaning between the resting state and the RDS[11]. **Eq. 3** therefore implicitly encodes for and depends on the existence of a single rate-determining step and a single (catalyst) resting state. In heterogeneous electrocatalysis, the resting state may manifest as active sites (*) being predominantly bare or, for example, saturated by adsorbed hydrogen atoms (H*). We note that **Eq. 3** also implicitly requires that confounding factors such as mass transport artifacts, ohmic losses, and active site restructuring are eliminated or appropriately accounted for.

For the past several decades, **Eq. 3** has been the cornerstone for kinetic and mechanistic study of interfacial ion transfer and corrosion processes[2,3] and electrocatalytic reactions including hydrogen evolution and oxidation (HER/HOR)[4,12], oxygen reduction and evolution (ORR/OER)[13,14], chlorine evolution (CER)[15,16], CO_2 and CO reduction[17–19], alkene epoxidation[20,21], and more[22,23]. Moreover, growing appreciation for the relevance of electrochemical elementary step events to thermochemical catalysis has led to invocation on **Eq. 3** to elucidate mechanisms and identify rate-determining steps during non-faradaic (i.e., thermochemical) reactions including formic acid dehydrogenation[24], CO_2 hydrogenation[25], and Brønsted-acid catalyzed alcohol dehydration[26]. In each of these contexts, mechanistic conclusions derived from observed Tafel slope are predicated on veracity of **Eq. 3** and its underpinning assumptions.

In addition to the aforementioned requirements for a single RDS and (catalyst) resting state, the fidelity of **Eq. 3** requires that all steps between the resting state and RDS are equilibrated (**Figure 1**). This condition—referred to as the pre-equilibrium approximation (PEA)—is necessary to ensure facile communication between the resting state and the RDS in the form of an *equilibrated* relay of $n_{pre-RDS}$ electrons for every σ_{RDS} traversals of the RDS. Importantly, these 'lines of communication' require that intervening elementary steps are equilibrated for the rate-determining step to 'speak with' the resting state. If pre-RDS steps are only partially reversible or even irreversible, then these 'lines of communication' are impeded and the additive factor of $n_{pre-RDS}/\sigma_{RDS}$ in **Eq. 3** is unjustified.

These limitations of **Eq. 3** have been recognized for OER electrocatalysis on IrO_2 and RuO_2 for which observed Tafel slopes commonly do not adhere to cardinal values—i.e., those predicted by **Eq. 3** for integer values of $n_{pre-RDS}$ and σ_{RDS}. Microkinetic modelling of OER mechanisms mediated by monatomic oxygen adatoms indicate that non-cardinal Tafel slopes result from breakdown of the PEA[27]. In spite of these findings, **Eq. 3** remains in ubiquitous use due to the lack of a more general alternative that quantifies the influence of pre-RDS *de*-equilibration on Tafel slope. This knowledge gap extends broadly across fields of catalysis and (interfacial) electrochemistry, representing a longstanding impasse to deepened mechanistic understanding of multi-step charge-transfer processes.

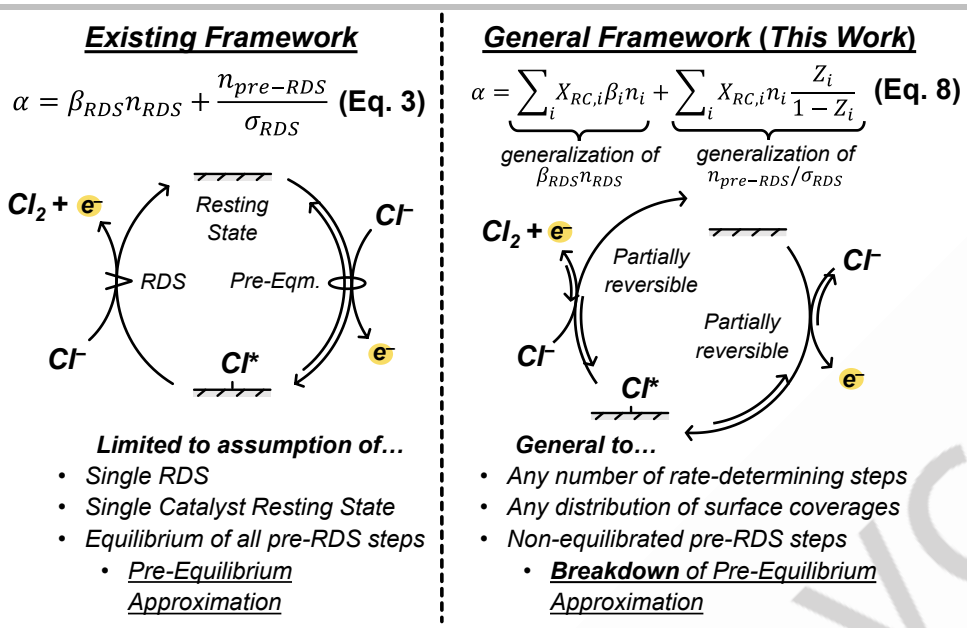

Figure 1. Mathematical descriptions of transfer coefficient (α) depicted through example of the chlorine evolution reaction (CER) proceeding via a Volmer-Heyrovský mechanism. The subscript RDS refers to the rate-determining step; β_{RDS}, σ_{RDS}, and n_{RDS} are respectively the symmetry factor of, stoichiometric number of, and the number of electrons transferred in the RDS; and, $n_{pre-RDS}$ is the number of electrons transferred 'before' the RDS—meaning between the resting state and the RDS. $X_{RC,i}$, Z_i, and n_i are respectively the degree of rate control, approach to equilibrium, and number of electrons transferred in step i. Mathematical definitions for $X_{RC,i}$ and Z_i are provided in **Eq. 4** and **Eq. 5** respectively.

In this Scientific Perspective, we ally the degree of rate control concept and principles of non-equilibrium thermodynamics to formulate a simple, universal equation that exactly quantifies the accuracy of the PEA and the consequences of its breakdown on the mechanistic interpretation of transfer coefficient and Tafel slope. In so doing, we also eliminate requirements of a single rate-determining step and/or resting state to formulate a general, closed-form expression for α (**Figure 1**). The general reformulation of **Eq. 3** developed herein is applied to energy-relevant case studies including the chlorine evolution reaction (CER) on Pt-Ir alloys and the oxygen reduction reaction (ORR) on iron phthalocyanine (FePc) catalysts. In each example, we reinterpret reported rate-potential dependencies to demonstrate that account of the approach to equilibrium of constituent elementary steps is critical to clarifying the mechanistic meaning of observed Tafel slope. In the case of the CER, we demonstrate that shifts in transfer coefficient (Tafel slope) from cardinal values of 1½ (40 mV/dec) to ½ (120 mV/dec) at low and high overpotential *do not* indicate a shift in the identity of the rate-determining step or the catalyst resting state. Instead, this transition in Tafel slope is a direct manifestation of the breakdown of the PEA—tracked quantitatively as a function of potential. We find that sufficiently large overpotentials (≳150 mV) result in a condition of *total faradaic irreversibility*—meaning that electrochemical bias has become so large as to drive all faradaic elementary steps (or molecular charge transfer events) to irreversibility. We surmise that this is, in fact, a general feature of multi-step charge transfer reactions that explains common observation of Tafel slopes which transition from ≤60 mV/dec to ~120 mV/dec with increasing overpotential. These same principles are demonstrated to reveal molecular-level origins of E-dependent transitions in Tafel slope during FePc-catalyzed ORR in potential regimes relevant for fuel cell applications and aerobic oxidation catalysis. In this case, we show that ORR Tafel slope—an ostensibly *electrochemical* descriptor—counter-intuitively quantifies the kinetic relevance of *chemical* O_2 activation. These findings highlight opportunities to elicit molecular-level detail even from E-dependent, non-cardinal Tafel slopes and are thus relevant for both traditional (electro)kinetic analysis and emerging practices including the analysis of Tafel slope plots[14,28,29] and study of mixed-potential-driven thermochemical catalysis[5,25,30–35]. Indeed, we leverage the developments in this work to enable a comparative analysis of rate–potential correlations during mixed-potential-driven aerobic oxidation catalysis on differently alloyed (Pt/C, PtCo/C, PtPd/C) and differently supported (Pt/SiO_2, Pt/Al_2O_3, Pt/TiO_2) catalysts. These analyses reveal that aerobic oxidation catalysis (i) operates in the regime of total faradaic irreversibility and (ii) proceeds through a competition of kinetically-relevant faradaic and non-faradaic elementary steps in a fashion apparently sensitive to support but not alloy identity. Throughout these case studies, conceptual learnings are critically enabled by explicit, quantitative connections made between Tafel slope and elementary step approach-to-equilibrium, which we contend is a key descriptor of multi-step charge transfer of comparable importance to rate-determining-step identity.

2. Kinetic and Thermodynamic Descriptors

We formulate a generalization of **Eq. 3** and assess the case studies to follow through descriptors which quantify the kinetic relevance and thermodynamic state of each elementary step. The kinetic relevance of an elementary step i is defined by the degree of rate control

$$X_{RC,i} \equiv \left(\frac{\partial \ln r}{\partial \ln k_{+i}}\right)_{K_i} = \frac{\partial \ln r}{\partial\left(-\frac{G^0_{TS,i}}{RT}\right)} \quad \textbf{(4)}$$

which quantifies the sensitivity of the overall net reaction rate (r) to changes in the forward rate constant of step i (k_{+i}) keeping the equilibrium constant (K_i) fixed[36–38]. In the context of transition state theory, $X_{RC,i}$ can be equivalently construed as the responsiveness of r to perturbations in the standard state free energy of the transition state, $G^0_{TS,i}$. Degrees of rate control for all steps in a catalytic cycle must sum to unity[36]; and, correspondingly, if there exists a single RDS, then $X_{RC,RDS} = 1$ and $X_{RC,j\neq RDS} = 0$. For sequences comprised of exclusively irreversible elementary steps, $X_{RC,i}$ is, alone, sufficient to describe the relevance of each step. However, in reactions with one or more reversible steps, non-rate-determining steps can affect reactivity through their influence on the concentration or surface coverage of intermediates. In these cases, the *thermodynamic* state, or approach to equilibrium, of each step must be quantified for a complete description of the influence of each step on the catalytic cycle[39,40].

The thermodynamic state of an elementary step i is quantified by the approach to equilibrium (Z_i), defined by the ratio of the rates in the reverse (r_{-i}) and forward (r_{+i}) directions:

$$Z_i \equiv \frac{r_{-i}}{r_{+i}} = e^{\frac{\Delta G_i}{RT}} \quad \textbf{(5)}$$

where ΔG_i is the free energy driving force for step i or, equivalently, the free energy deviation of step i from an equilibrated state. We note that ΔG_i as defined in **Eq. 5** is *inclusive* of electrochemical contributions and is therefore a function of E. The approach to equilibrium (Z_i) is equal to unity for a fully reversible, or equilibrated, step and approaches zero for an irreversible step. Z_i is therefore *the* salient parameter for quantifying the 'approach to accuracy' of the pre-equilibrium approximation. In order to formulate general corrections to the pre-equilibrium $n_{Pre-RDS}/\sigma_{RDS}$ term in **Eq. 3** for cases where $Z_{Pre-RDS} \neq 1$, we must consider the kinetic significance of both forward ($+i$) and reverse ($-i$) *half*-steps. To do so, we define half-step analogs of the degree of rate control, referred to as reaction sensitivities:

$$s_{\pm i} \equiv \frac{\partial \ln r}{\partial \ln k_{\pm i}} \quad \textbf{(6)}$$

which are similar to $X_{RC,i}$ except K_i is not fixed (i.e., k_{+i} and k_{-i} are varied independently). Accordingly, $s_{\pm i}$ are the forward and reverse contributions to degree of rate control (i.e., $X_{RC,i} = s_{+i} + s_{-i}$) and are subject to thermodynamic constraints analogously to elementary half-step rates (i.e., $Z_i = -s_{-i}/s_{+i}$ analogous to $Z_i = r_{-i}/r_{+i}$ per **Eq. 5**). The specificity of $s_{\pm i}$ to each elementary *half*-step is particularly enabling for connecting microscopic descriptors (i.e., symmetry factor, β_i) to macroscopic observables (i.e., transfer coefficient, α) with account of elementary step approach to equilibrium (i.e., approach to PEA validity).

3. Results and Discussion

The foregoing descriptors provide a framework to recast α in explicit terms of elementary step symmetry factors (β_i). Following the developments of Foley and Bhan[36,41], macroscopic observables such as α are equal to the $s_{\pm i}$-weighted average of their half-step analogs. In this case,

$$\alpha = \sum_{+i} \beta_i n_i \times s_{+i} - \sum_{-i} (1-\beta_i) n_i \times s_{-i} \quad \textbf{(7)}$$

where $\beta_i n_i$ is the 'transfer coefficient' of the forward half-step $+i$ and $-(1-\beta_i)n_i$ is the 'transfer coefficient' of the reverse half-step $-i$. This reconstrual of α in terms of $s_{\pm i}$ and β_i is general to any reaction sequence and readily admits temperature- or potential-dependent β_i that manifest in, for example, enthalpic/entropic formulation of β[42,43] or quantum mechanical treatments of electron transfer such as Marcus-Hush-Chidsey theory[10,38,44,45]. Section S1 and Section S2 respectively provide discussion of temperature- and potential-dependent symmetry factors analyzed through the framework developed in this work. However, in order to maintain our focus on scrutiny of the PEA and generalization of **Eq. 3**, we limit this Scientific Perspective to discussion of constant β_i.

As we detail in Section S3, combination of **Eq. 7** with aforementioned relationships between $s_{\pm i}$, $X_{RC,i}$, and Z_i produces a single, general expression for α in terms of the kinetic ($X_{RC,i}$) and thermodynamic (Z_i) relevance of elementary steps

$$\alpha = \sum_{steps} X_{RC,i} n_i \left(\beta_i + \frac{Z_i}{1-Z_i}\right) = \underbrace{\sum_i X_{RC,i}\beta_i n_i}_{\substack{generalization\ of \\ \beta_{RDS}n_{RDS} \\ in\ \textbf{Eq. 3}}} + \underbrace{\sum_i X_{RC,i} n_i \frac{Z_i}{1-Z_i}}_{\substack{generalization\ of \\ n_{pre-RDS}/\sigma_{RDS} \\ in\ \textbf{Eq. 3}}} \quad \textbf{(8)}$$

Eq. 8 reveals that transfer coefficients are $X_{RC,i}$-weighted averages of both the potential-dependence (β_i) and thermodynamic state ($Z_i(1-Z_i)^{-1}$) of each elementary step. Crucially, these averages are precise generalizations of the $\beta_{RDS}n_{RDS}$ and $n_{pre-RDS}/\sigma_{RDS}$ terms in **Eq. 3**. The rightmost side of **Eq. 8** shows that $\beta_{RDS}n_{RDS}$ and $n_{pre-RDS}/\sigma_{RDS}$ terms from **Eq. 3** are 'broadened' to account for any distribution of rate control ($X_{RC,i}$) and any approach-to-(pre)equilibrium (Z_i). In this sense, **Eq. 8** is faithfully viewed as a formal generalization of the familiar 'cardinal' formula for transfer coefficient. Indeed, we show in Section S4 that **Eq. 8** simplifies to the limiting form of **Eq. 3** for the special conditions listed in **Figure 1**—i.e., that there is a single RDS and resting state and the PEA is valid.

We note that the approach of recasting α in terms of $X_{RC,i}$ and Z_i (e.g., **Eq. 8**) to obtain general formulae is not unique to transfer coefficient and can be readily extended to complementary kinetic observables including reaction order and activation energy. Although these treatments are beyond the scope of this Scientific Perspective, the mathematical framework developed herein may be used as a model for the employ of $X_{RC,i}$ and Z_i concepts to guide interpretation of *any* kinetic observable in the context of multi-step charge transfer reactions.

As we discuss hereinbelow, **Eq. 8** generally describes potential-dependent transfer coefficients both near and far from equilibrium. Crucially, however, measurement of α near equilibrium conflates contributions of the forward and reverse (or anodic and cathodic) reaction paths. Historically, the influence of potential on the *forward* current density has been extracted by 'subtracting off' the 'backwards current' from the measured *net* current density[46]. We generalize this approach through quantification of the *forward* transfer coefficient ($\vec{\alpha}$) in terms of α and a thermodynamic correction term per **Eq. 9**:

$$\vec{\alpha} \equiv \frac{RT}{F}\frac{\partial \ln \vec{r}}{\partial E} = \alpha - \frac{n\prod_i Z_i}{1-\prod_i Z_i} \quad \textbf{(9)}$$

Derivation of **Eq. 9** and an analogous expression for $\overleftarrow{\alpha}$ are provided in Section S5. We reiterate that **Eq. 9** in tandem with **Eq. 8** is necessary to establish a description of transfer coefficient (or Tafel slope) that appropriately 'subtracts off' the contribution of reverse rates near equilibrium.

3.1 Case Study I: Chlorine Evolution Reaction (CER) on Pt-Ir Alloys

We showcase the utility of **Eq. 8** to describe mechanistic origins of E-dependent Tafel slope through examination of polarization curves for the chlorine evolution reaction (CER) on Pt-Ir alloys reported by Tilak[46]. Measurements of steady-state forward CER current densities in Cl_2-saturated 5 M NaCl at 95°C are shown in **Figure 2** as a function of applied overpotential (i.e., E versus the Cl_2/Cl^- equilibrium potential measured at open-circuit conditions). Forward CER current densities ($\vec{J}_{CER}$) are calculated by Tilak[46] by correcting for the reverse reaction as a function of overpotential per **Eq. 10**:

$$\vec{J}_{CER} = \frac{J_{CER}}{1 - e^{\frac{-2FE}{RT}}} \quad \textbf{(10)}$$

which implicitly assumes that (i) activities of Cl_2 and Cl^- are constant and (ii) all kinetically-relevant steps have a stoichiometric number of unity. Accordingly, Tilak proposes a two-step Volmer-Heyrovský mechanism shown in **Table 1** wherein Cl^- electrochemically adsorbs to form Cl* (Volmer) and subsequently reacts with a second, fluid-phase Cl^- through concerted electron transfer to form Cl_2 (Heyrovský). For low overpotential ($E \lesssim 60$ mV vs Cl_2/Cl^-), the reverse reaction rate is appreciable and therefore, $\vec{\alpha}_{CER}$ is not equal to α_{CER}. In this near-equilibrium regime, **Eq. 9** must be used to relate α_{CER} to $\vec{\alpha}_{CER}$ based on elementary step reversibilities (Z_i). We note that for $E \gtrsim 60$ mV vs Cl_2/Cl^-, the reverse reaction rate is negligible and thus $\vec{\alpha}_{CER} \approx \alpha_{CER}$.

Table 1: Volmer-Heyrovský mechanism and regressed kinetic parameters for chlorine evolution on Pt-Ir alloys

	Step	σ_i	k_{+i}† / mA cm^{-2}	k_{-i}† / mA cm^{-2}	β_i
Volmer (V)	$Cl^- + * \rightleftharpoons Cl^* + e^-$	1	76	3800	0.40
Heyrovský (H)	$Cl^- + Cl^* \rightleftharpoons Cl_2 + * + e^-$	1	40	0.80	0.62

†Rate constants are potential-independent and defined at the Cl_2/Cl^- equilibrium potential at 95°C with 1 bar Cl_2 and 5 M NaCl. Kinetic parameters are reported with two significant figures.

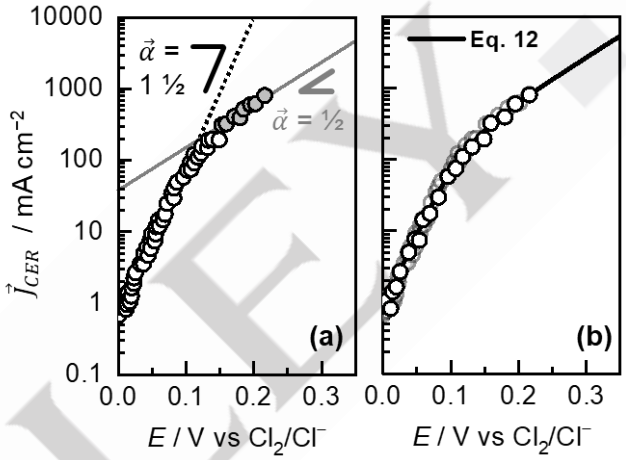

Figure 2. Steady-state forward current density of chlorine evolution reaction ($\vec{J}_{CER}$) on Pt-Ir alloy electrodes at 95°C with 1 bar Cl_2 and 5 M NaCl measured by Tilak[46]. **(a)** Steady-state rate measurements (○, ○) are colored in correspondence with linear Tafel regimes described by $\vec{\alpha}_{CER}$ = 1 ½ (**- - -**) and $\vec{\alpha}_{CER}$ = ½ (**—**). **(b)** Steady-state rate measurements (○) are compared to Volmer-Heyrovský mechanism per **Eq. 12** (**—**) and regressed kinetic parameters reported in **Table 1**. A random selection of experimental data are grayscaled (○) and placed behind prediction of **Eq. 12** (**—**) to aid visual inspection of goodness-of-fit.

Figure 2(a) shows that, for $E \lesssim 60$ mV, the forward rate (or current) of CER scales with potential according to a log-linear relationship such that $\vec{\alpha}_{CER} \approx$ 1½ (shown by - - - in **Fig. 2(a)**). Following **Eq. 3** and the left panel of **Figure 1**, these observations indicate that CER proceeds via rate-determining Cl_2 formation preceded by equilibrated electrosorption of Cl^- onto a vacant site—which is the catalytic resting state. As overpotential increases beyond ~60 mV, the overall reaction becomes unidirectional (i.e., irreversible), and the transfer coefficient gradually transitions to another cardinal value $\vec{\alpha}_{CER} = \alpha_{CER} \approx$ ½ for $E \gtrsim 150$ mV (shown by — in **Fig. 2(a)**). According to the pre-equilibrium approximation and **Eq. 3**, this indicates either (i) a transition in the RDS from the Volmer step to the Heyrovský step or (ii) a transition in the resting state from * to Cl*. We suggest that, in fact, neither of these conventional interpretations is correct. Instead, increasing electrochemical bias drives each electrochemical step to de-equilibrate and become irreversible (i.e., $Z_i \ll 1$ for all i with $n_i \neq 0$). Substituting this condition into **Eq. 8** specifies

$$\alpha = \sum_{\substack{i \\ steps}} X_{RC,i} n_i \left(\beta_i + \frac{Z_i}{1 - Z_i}\right) \underset{for\ all\ i}{\overset{Z_i \ll 1}{\Longrightarrow}} \sum_{\substack{i \\ steps}} X_{RC,i} n_i \beta_i \approx {}^1/_2 \quad \textbf{(11)}$$

regardless of the identity of kinetically-relevant steps and most abundant surface intermediates. That is to say that, in this irreversible regime, the transfer coefficient will be ~½ for *any* distribution of surface coverage (θ_{j^*}) and degree of rate control ($X_{RC,i}$). This condition is general to any mechanism in which all kinetically-relevant steps are faradaic and, therefore, provides an explanation for the frequent observation of α (b) which transition from > 1 (< 60 mV dec^{-1} at 298 K) at low overpotential to ~½ (~120 mV dec^{-1} at 298 K) at high overpotential.

In order to explicate this phenomenon in more detail, we fit the data in **Figure 2(a)** to **Eq. 12**, a closed-form expression for $\vec{j}_{CER}$ derived by application of the steady-state condition to Cl*, as detailed in Section S6:

$$\vec{j}_{CER} = \frac{k_{+V}k_{+H}a_{Cl^-}^2 e^{\frac{F(\beta_V+\beta_H)E}{RT}} - k_{-V}k_{-H}P_{Cl_2}e^{\frac{-F(2-\beta_V-\beta_H)E}{RT}}}{k_{+V}a_{Cl^-}e^{\frac{F\beta_V E}{RT}} + k_{-V}e^{\frac{-F(1-\beta_V)E}{RT}} + k_{+H}a_{Cl^-}e^{\frac{F\beta_H E}{RT}} + k_{-H}P_{Cl_2}e^{\frac{-F(1-\beta_H)E}{RT}}} \times \frac{1}{1-Z_V Z_H} \quad \textbf{(12)}$$

The corresponding kinetic parameters, determined by non-linear regression, are reported in **Table 1** and are shown in **Figure 2(b)** (**—**) to agree well with experimental rate data. Based on this simple kinetic model, we calculate E-dependent forward transfer coefficients ($\vec{\alpha}_{CER}$), elementary step reversibilities (Z_i), degrees of rate control ($X_{RC,i}$), and surface coverages (θ_{j^*}) shown in **Figure 3**. As shown in **Figure 3(a)**, forward transfer coefficients calculated by differentiation of **Eq. 12** are in quantitative agreement with **Eq. 8** and **Eq. 9** developed in this work—evincing the accuracy of our general formulation for transfer coefficient. Moreover, **Figure 3(a)** confirms that $\vec{\alpha}_{CER} \approx 1½$ for $E \leq 60$ mV vs Cl$_2$/Cl$^-$. In the same potential regime, **Figure 3(b)-(c)** show that $Z_V \approx 1$, $X_{RC,H} \approx 1$, and $\theta_* \approx 1$—meaning that the Volmer step is (pre)equilibrated, the Heyrovský step is rate-determining, and the catalyst resting state is a bare surface. Therefore, for $E \lesssim 60$ mV, the conventional pre-equilibrium paradigm embodied by **Eq. 3** and the left panel of **Figure 1** faithfully describes the CER mechanism.

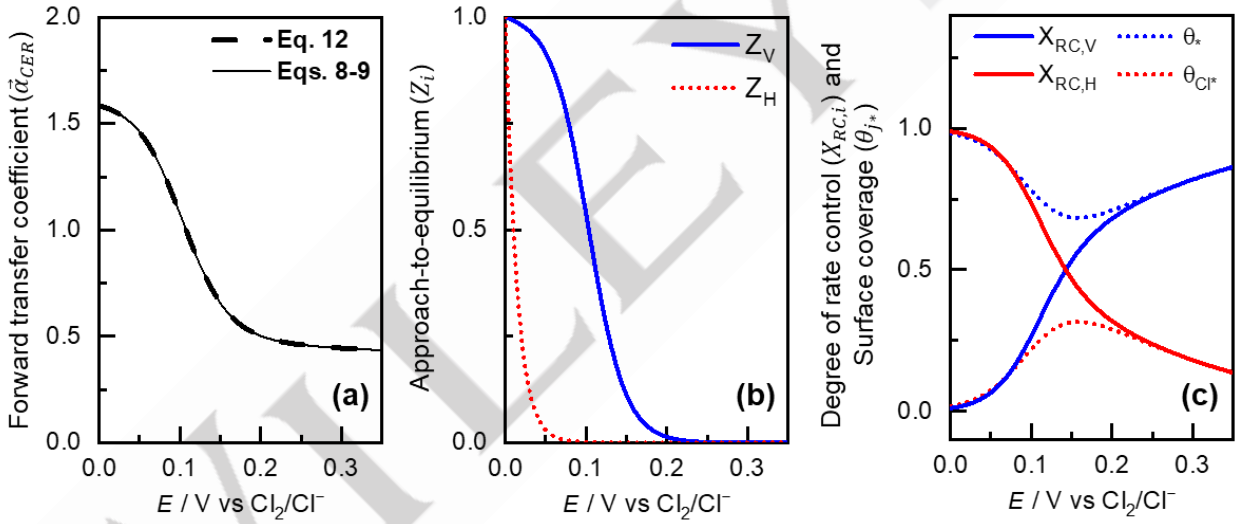

Figure 3. Steady-state kinetic descriptors of the chlorine evolution reaction (CER) calculated per the Volmer-Heyrovský mechanism and regressed parameters reported in **Table 1**. **(a)** Forward CER transfer coefficient ($\vec{\alpha}_{CER}$) calculated by differentiation of **Eq. 12** (**– –**) or **Eqs. 8-9** (—) derived in this work. **(b)** Approach-to-equilibrium, or reversibility, of the Volmer step (Z_V, **—**) and Heyrovský step (Z_H, **•••**) calculated per the definition in **Eq. 5**. **(c)** The degree of rate control of the Volmer step ($X_{RC,V}$, **—**) and Heyrovský step ($X_{RC,H}$, **—**) and the surface coverage of vacant sites (θ_*, **•••**) and adsorbed chlorine (θ_{Cl^*}, **•••**).

Examination of elementary step rate constants reported in **Table 1** reveals that the forward rate constants of the Volmer step ($k_{+V} = 76$ mA cm^{-2}) and Heyrovský step ($k_{+H} = 40$ mA cm^{-2}) are similar. Therefore, Volmer pre-equilibrium is *not* due to faster intrinsic kinetics of the forward Volmer step relative to the forward Heyrovský step. Instead, the Volmer step equilibrates because the *reverse* step is facile (i.e., $k_{-V} \gg k_{+H}, k_{+V}$). However, increase in E beyond ~60 mV biases CER in the anodic (forward) direction to such an extent that even the reverse Volmer step becomes slow relative to the forward Volmer and Heyrovský steps (i.e., $r_{-V} < r_{+H}, r_{+V}$ despite $k_{-V} \gg k_{+H}, k_{+V}$). Once $E \gtrsim 150$ mV vs Cl$_2$/Cl$^-$, the Volmer step becomes irreversible, indicated by $Z_V \ll 1$ in **Figure 3(b)**. This transition in Z_V reflects a breakdown of the pre-equilibrium approximation and establishment of total irreversibility, resulting in $\vec{\alpha}_{CER} \approx ½$ shown in **Figure 3(a)** and predicted by **Eq. 11** for $Z_V, Z_H \ll 1$.

Achievement of total irreversibility for $E \gtrsim 150$ mV vs Cl_2/Cl^- can also be understood through inspection of E-dependent reaction coordinate diagrams. **Figure 4** shows potential energy surfaces calculated at equilibrium (E = 0 V vs Cl_2/Cl^-; —) and near the onset of total irreversibility (E = 0.2 V vs Cl_2/Cl^-; —) assuming a transition state theory formulation of half-step rates. Details regarding calculation of (electro)chemical potential energies are reported in Section S7. At the Cl_2/Cl^- equilibrium potential (—), the energy barrier for the reverse Volmer step (~60 kJ/mol) is significantly smaller than for the forward Heyrovský step (~74 kJ/mol). This ~14 kJ/mol difference in energy barrier amounts to a exp[~14 kJ/mol×(RT)$^{-1}$] ≈ 100× ratio in rate constant—consistent with k_{-V} and k_{+H} reported in **Table 1**. The relative kinetic sluggishness of the forward Heyrovský step results in a robust Volmer step pre-equilibrium at low overpotential, as reported in **Figure 3(b)**. Increase of potential to E = 0.2 V vs Cl_2/Cl^- (—) biases all steps in the forward (anodic) direction, reflected by stabilization of all intermediate, transition, and product states in **Figure 4**. The magnitude of stabilization increases with the number of electrons transferred relative to the reactant state. Consequently, the barrier for the reverse Volmer step and forward Heyrovský step respectively *increase* and *decrease* by ~½F × 0.2 V ≈ 12 kJ/mol. These opposing effects result in the previously sluggish Heyrovský step outpacing the decelerated reverse Volmer step in competitive removal of Cl*. As a result, Cl* reacts predominantly through the forward Heyrovský step and the reverse Volmer step becomes insignificant—in other words, the Volmer step becomes *irreversible*, as seen in **Figure 3(b)**.

These consequences of increasing potential are not unique to the particular potential energy surface (PES) for CER on PtIr alloys but are general to all electrocatalytic reactions and any electrocatalytic surface. Although each metal or metal alloy catalyst will possess a unique PES, the phenomenon of asymmetric bias induced by E is universal. For each electrocatalyst, the potential required for onset of total irreversibility will depend on, for example, the relative barrier heights of the forward Heyrovský step and the reverse Volmer step. These differences in barrier height typically correlate with intermediate binding energies and therefore catalyst composition through linear free-energy scaling relations well-established in surface (electro)catalysis[47,48]. As a consequence, we anticipate that measurement of overpotentials which induce total faradaic irreversibility may provide a pathway to formulating PESs across a suite of materials in a fashion complementary to computational methods (e.g., density functional theory).

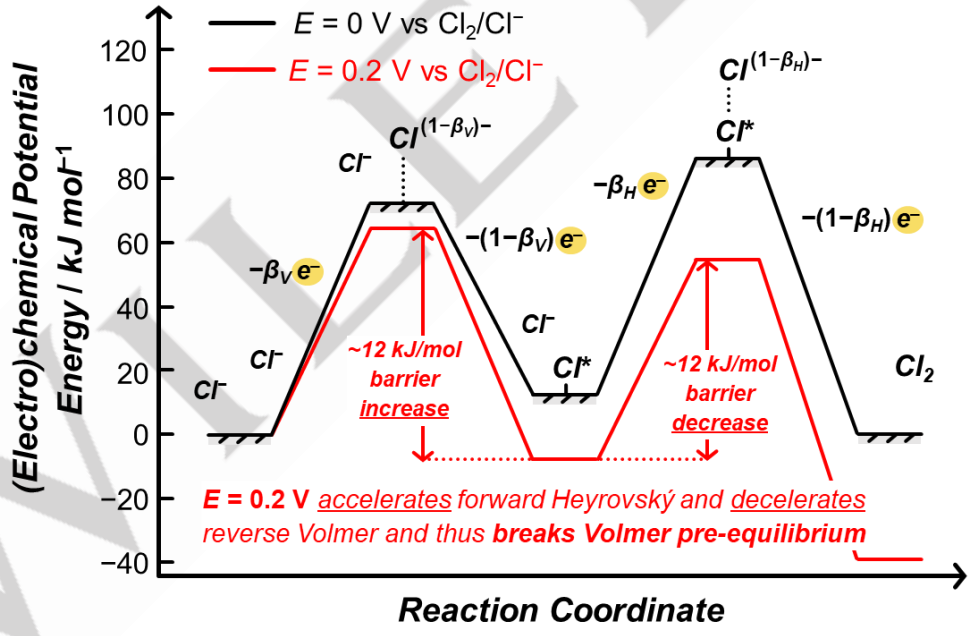

Figure 4. Potential energy reaction coordinate diagram of the Volmer-Heyrovský mechanism for the chlorine evolution reaction (CER) at E = 0 V vs Cl_2/Cl^- (—) and E = 0.2 V vs Cl_2/Cl^- (—) per the kinetic parameters reported in **Table 1**. Electrochemical potential energies are calculated assuming a transition state theory formulation of $k_{\pm i}$ and according to potential-dependence of each half-step prescribed by β_i. Further calculation details are provided in Section S7.

For each catalyst surface, the inevitable state of total irreversibility means that only *forward* half-steps contribute to the measured transfer coefficient. In the context of CER, this implies $\vec{\alpha}_{CER} = \alpha_{CER} \approx ½$ regardless of the distribution of rate control amongst the Volmer and Heyrovský step—as is reflected in **Figure 3(a)**. Modest

variations in $\vec{\alpha}_{CER}$ between 0.45 and 0.55 for $E \gtrsim 150$ mV vs Cl_2/Cl^- in **Figure 3(a)** are due to asymmetry in regressed symmetry factors (β_V = 0.40 and β_H = 0.62 in **Table 1**). However, in experimental contexts, transfer coefficients between 0.45 and 0.55 (or Tafel slopes between 110 mV dec^{-1} and 133 mV dec^{-1} at 298 K) are within typical measurement error and are unlikely to be distinguishable with sufficient confidence to discriminate between two candidate rate-determining steps. Therefore, although the condition of $\alpha \approx ½$ in the totally irreversible regime is general to any catalyst composition, this observation provides *no information* regarding the relative kinetic relevance of electrochemical steps (e.g., the Volmer *vs* Heyrovský step). In other words, the measurement of 'cardinal' transfer coefficients of $\alpha \approx ½$ cannot be interpreted as a signature of a particular rate-determining charge transfer step since $\alpha \approx ½$ is consistent with *any* distribution of rate control amongst electrochemical steps. This mechanistic information is not lost but instead manifests in surface coverage rather than transfer coefficient or Tafel slope. In the case that each elementary step is irreversible, surface-bound intermediates can only be removed by forward half-steps. As a result, species such as Cl* accumulate in exact correspondence with the kinetic sluggishness—or rate-determining character—of the forward half-steps which remove them. Stated mathematically for the case of the CER mechanism in **Scheme 2**,

$$X_{RC,V} = \theta_* \tag{13}$$

and

$$X_{RC,H} = \theta_{Cl^*} \tag{14}$$

Eqs. 13-14 are derived in generality under the condition of total irreversibility in Section S8. The congruence of surface coverage and degree of rate control within the totally irreversible regime specified by **Eqs. 13-14** is illustrated in **Figure 3(c)**. Volmer pre-equilibrium at low overpotential ($E \lesssim 60$ mV) allows for maintenance of a low steady-state Cl* surface coverage (i.e., $\theta_{Cl^*} \ll 1$) despite forward Cl* removal being the rate-determining step (i.e., $X_{RC,H} \approx 1$). However, as overpotential is increased to the totally irreversible regime ($E \gtrsim 150$ mV), the Volmer step de-equilibrates and Cl* necessarily accumulates in accordance with the degree of rate control of Cl* removal (i.e., $\theta_{Cl^*} = X_{RC,H}$ per **Eq. 14**). Stated another way, because Cl* can only be removed through the forward Heyrovský step, the 'sluggishness' (or degree of rate control) of Cl* removal dictates the 'degree of accumulation' (or surface coverage) of Cl*. As we show in Section S8, this is a general principle of sequences of irreversible elementary steps and therefore a general principle of electrocatalytic reactions in the regime of total irreversibility. Crucially, however, since k_{+H} and k_{+V} are comparable, neither step is wholly rate-determining and, therefore, neither species dominates the surface. Both the Volmer and Heyrovský step maintain appreciable rate control for E = 200–350 mV vs Cl_2/Cl^-. Within this potential regime, the partitioning of rate control between the Volmer and Heyrovský step (i) has no measurable influence on transfer coefficient and (ii) is exactly reflected by the distribution of * and Cl*. Therefore, in the large overpotential regime ($E \gtrsim 150$ mV), surface coverage—rather than Tafel slope or transfer coefficient—is a diagnostic reporter of degree of rate control.

Based on these findings, we advocate for quantification of adsorbate surface coverage as a kinetic measurement complementary to transfer coefficient. Surface coverage can be quantified through voltammetry[49,50], spectroscopic methods[51,52], open-circuit potential decay transients[53], and emerging techniques such as electrochemical steady-state isotopic transient kinetic analysis (eSSITKA)[54]. Quantification of surface coverage through these methods provides a uniquely step-specific signature of the degree of rate control—particularly if $\alpha \approx ½$ is observed at large overpotential (e.g., **Eqs. 13-14**). We acknowledge, however, that measurement of adsorbate surface coverage is challenging at catalytic solid-liquid interfaces and may be near-impossible with instrumentation commonly available to electrocatalysis practitioners. In these scenarios, the measurement of reaction order offers a straightforward alternative which probes the involvement of fluid-phase species (e.g., Cl^-) in kinetically-relevant and/or 'pre-RDS' steps—as has been thoroughly discussed in the context of faradaic and non-faradaic catalysis[36,38]. Reaction order measurements represent a natural complement to transfer coefficient, particularly near equilibrium where the pre-equilibrium approximation is reliable and predicts integer reaction orders that can distinguish between competing mechanistic proposals[4,55]. Unfortunately, in the case of the CER mechanism in **Scheme 2**, the identical participation of one chloride ion in each step results in a first-order dependence on Cl^- concentration irrespective of the distribution of rate-control in the totally irreversible kinetic regime. For this reason, surface coverage is, in many scenarios, privileged with unparalleled step-specificity which contrasts integer reaction orders and half-integer transfer coefficients which may be unreliable indicators of rate-determining step identity far from equilibrium. This maxim is particularly important for measurement and interpretation of transfer coefficient given the patent propensity of electrocatalytic reactions to display $\alpha \geq 1$ ($b \leq 60$ mV dec^{-1} at 298 K) at low overpotential which transition to $\alpha \approx ½$ ($b \approx 120$ mV dec^{-1} at 298 K) at high overpotential. These so-called 'double Tafel slopes'[56] appear frequently, as we demonstrate by a collation of three such examples in **Figure 5**.

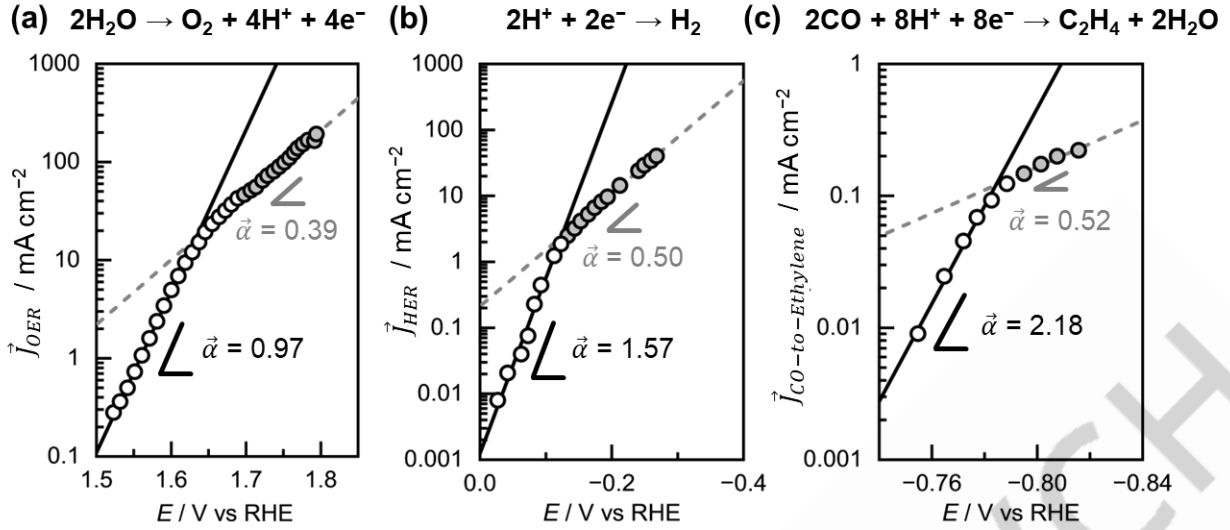

Figure 5. Steady-state forward current density of **(a)** the oxygen evolution reaction (OER) on IrO_2–Ta_2O_5 electrodes in 0.5 M H_2SO_4 at 25°C[57], **(b)** the hydrogen evolution reaction (HER) on Ni-Mo-Cd electrodes in 1.0 M NaOH at 5°C[58], **(c)** CO reduction to C_2H_4 on Cu electrodes in phenol/phenoxide-promoted dimethyl sulfoxide (DMSO) at 25°C[19]. In each panel, two distinct linear Tafel regimes are identified at low (○, —) and high (●, - - -) overpotential. Transfer coefficients are determined by linear regression of the shown steady-state polarization data.

Figure 5(a-c) shows steady-state polarization curves for **(a)** acidic OER on IrO_2–Ta_2O_5 anodes[57], **(b)** alkaline HER on Ni-Mo-Cd cathodes[58], and **(c)** CO reduction to C_2H_4 on Cu cathodes in phenol/phenoxide-promoted dimethyl sulfoxide (DMSO) solvent[19]. In each case, forward current densities scale in a log-linear fashion with respect to applied potential (E) with distinct regimes at low overpotential (○) and high overpotential (●). At low overpotential, forward transfer coefficients are **(a)** $\vec{\alpha} \approx 1$ for OER, **(b)** $\vec{\alpha} \approx 1\frac{1}{2}$ for HER, and **(c)** $\vec{\alpha} \approx 2$ for CO reduction to C_2H_4. These observations are interpreted per **Eq. 3** to respectively indicate **(a)** a rate-determining chemical step ($\beta_{RDS}n_{RDS} = 0$) preceded by a single pre-equilibrium electron transfer ($n_{pre-RDS}/\sigma_{RDS} = 1$), **(b)** a rate-determining electrochemical step ($\beta_{RDS}n_{RDS} = \frac{1}{2}$) preceded by a single pre-equilibrium electron transfer ($n_{pre-RDS}/\sigma_{RDS} = 1$), and **(c)** a rate-determining chemical step ($\beta_{RDS}n_{RDS} = 0$) preceded by two successive pre-equilibrium electron transfers ($n_{pre-RDS}/\sigma_{RDS} = 2$). At high overpotential, these distinct rate-potential dependencies vanish and $\vec{\alpha} = \alpha \approx \frac{1}{2}$ for each reaction.

For each case in **Figure 5**, transition to $\vec{\alpha} \approx \frac{1}{2}$ is consistent with **Eq. 11** and thus plausibly reflects a breakdown of the pre-equilibrium approximation resulting in **(a,c)** a shift in rate control from a chemical step to previously equilibrated but now irreversible electrochemical step(s) and **(b)** de-equilibration of pre-RDS step(s) which exhibit indeterminate rate control akin to the case of Volmer de-equilibration in **Figure 3**. These analyses suggest that PEA breakdown provides a general explanation of commonly observed transitions to $\vec{\alpha} \approx \frac{1}{2}$ at large overpotential and, therefore, must be considered in mechanistic study of electrocatalytic reactions far from equilibrium. Moreover, we highlight that the overpotentials which lead to transition to $\vec{\alpha} \approx \frac{1}{2}$ are typically ~150 mV relative to the onset potential (see **Figure 3** and **Figure 5**)—indicating that even 'modest' overpotentials commonly encountered in electrokinetic studies are prone to total irreversibility.

We do not mean to claim that $\vec{\alpha} \approx \frac{1}{2}$ *necessarily* indicates PEA breakdown; rather, we emphasize that elementary-step reversibility (Z_i) provides a quantitative measure of potential-driven dynamics which is intimately connected to transfer coefficient (**Eqs. 8-9**) and profoundly influences both rate-determining step identity and surface coverage (**Eqs. 13-14**). Indeed, the conceptual and mathematical framework provided by explicit consideration of Z_i informs mechanistic interpretation even in cases wherein robust pre-equilibrium can be maintained over broad potential ranges due to large asymmetries in elementary step rate constants. To illustrate such an example, we show in Section S9 that arbitrary decrease of k_{+H} and k_{-H} in **Table 1** by 1000× results in a more robust Volmer pre-equilibrium and in transition of $\vec{\alpha}_{CER}$ from ~1½ to ~½ before the condition of total irreversibility is achieved. In this special case, Volmer pre-equilibrium is maintained over a broader potential range because of a large kinetic asymmetry in the reverse Volmer step and forward Heyrovský step (i.e., $\frac{k_{-V}}{k_{+H}} \approx 10^5$). Even with this difference, the pre-equilibrium approximation breaks down for $E \gtrsim \log_{10}\frac{k_{-V}}{k_{+H}} \times \ln(10)RT/F$ = 365 mV and

potential-driven evolutions in degree of rate control and surface coverage emerge in correspondence with **Eqs. 13-14**—with $\vec{\alpha}_{CER}$ ~½ throughout the regime of total irreversibility.

In addition, we note that increasing overpotential can, in principle, lead to an increase in α rather than the monotonic decrease observed in all preceding examples. Based on our examination of reported polarization curves, instances of α increasing with overpotential are very rare. These unconventional $E-\alpha$ trends can result from interconnected reaction networks that involve competing pathways to multiple products, and which may be further complicated by a diversity of active sites on heterogeneous surfaces. We detail one such example in the case of competing CO reduction and H_2 evolution on polycrystalline Cu in EtOH solvent in Section S10[17]. In this case, α_{HER} transitions from ~0.2 to ~2 with increasing overpotential. Briefly, these 'inverted' transitions in α_{HER} plausibly emerge due to competition between CO* and H* and the known site diversity of Cu cathodes. Site diversity is hypothesized to result in distinct populations of reactive hydrogen adatoms that are non-competitive with CO at low overpotential (α_{HER} ~ 0.2; CO reaction order ~ 0) and competitive with CO at high overpotential (α_{HER} ~ 2; CO reaction order = −2) in a fashion consistent with observed CO reaction orders and the present framework for interpretation of α in terms of elementary-step descriptors. In addition to these 'inverted' transitions in transfer coefficient, increasing overpotential can also induce α that do not approach cardinal values and instead monotonically decrease *below* ~½ due to the competing kinetic relevance of chemical and electrochemical steps. In the following, we explicate these phenomena in the context of non-cardinal transfer coefficients observed during oxygen reduction on earth-abundant molecular catalysts.

3.2 Case Study II: Oxygen reduction on Iron-Phthalocyanine

Electrocatalytic reduction of O_2 to H_2O is an energy-relevant reaction that occurs via multi-step mechanisms comprised of several candidate rate-determining steps and kinetically-relevant surface intermediates[56]. These complexities are reflected in common observation of potential-dependent transfer coefficient/Tafel slope which challenge mechanistic interpretation through existing formalisms (i.e., **Eq. 3**)—as has also been highlighted for the reverse reaction, oxygen evolution[27]. We apply the foregoing developments to describe and interpret E-dependent Tafel slopes of ORR on carbon-supported iron phthalocyanine (FePc) catalysts per the mechanistic sequence (**Figure 6**) and corresponding kinetic parameters (**Table 2**) determined via a combination of steady-state and transient voltametric methods[59].

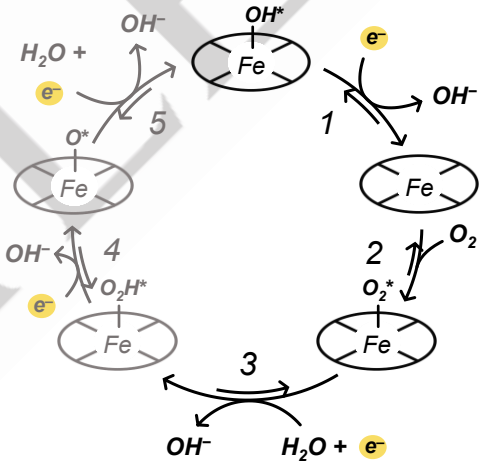

Figure 6. Catalytic cycle for the oxygen reduction reaction (ORR) on carbon-supported iron phthalocyanine (FePc/C) in 0.1 M KOH proposed by Elbaz and coworkers[59]. The greyed steps (steps 4 and 5) are determined to be kinetically-irrelevant at all conditions (i.e., for E = 0.55–1.0 V vs RHE). The top-most catalytic state, OH*, is the resting state near the onset potential (E = 1.0 V vs RHE).

Table 2. Mechanism of oxygen reduction reaction (ORR) on carbon-supported iron phthalocyanine (FePc/C) in 0.1 M KOH and regressed kinetic parameters reported by Elbaz and coworkers[59].

	Step	σ_i	k_{+i}† / s^{-1}	E_i^0† / V vs RHE	β_i
1	$OH^* + e^- \rightleftharpoons OH^- + *$	1	60	0.82	½
2	$O_2 + * \rightleftharpoons O_2^*$	1	2000	n/a	n/a
3	$O_2^* + H_2O + e^- \rightleftharpoons O_2H^* + OH^-$	1	3	1.09	½
4	$O_2H^* + e^- \rightleftharpoons O^* + OH^-$	1	>0.01	1.65	½
5	$O^* + H_2O + e^- \rightleftharpoons OH^* + OH^-$	1	>0.01	1.38	½

†Forward rate constants (k_{+i}) are potential-independent and defined at the equilibrium potential of the corresponding step (E_i^0) rather than the O_2/H_2O equilibrium potential at working conditions (1.23 V vs RHE at 25°C with 1 bar O_2 and in 0.1 M KOH). RHE refers to the reversible hydrogen electrode. k_{-i} are determined per k_{+i} and E_i^0. For step 2, k_{-2} = 3333 s^{-1} is potential-independent. Reaction kinetics are insensitive to k_{+4} and k_{+5} for the stated values as reported by Elbaz and coworkers[59].

The regressed elementary-step rate constants and equilibrium potentials in **Table 2** are shown by Elbaz and coworkers to produce steady-state and transient current-potential relationships which agree well with experimental observations for E = 0.55–1.0 V vs RHE in O_2-saturated 0.1 M KOH—conditions for which O_2 reduction produces H_2O with negligible formation of H_2O_2 byproduct[59]. In order to establish a kinetic understanding of FePc-catalyzed ORR at these conditions, we calculate steady-state α_{ORR} by (i) numerical differentiation of current with respect to potential (**Eq. 2**) and (ii) using foregoing formalisms that leverage elementary-step reversibility (Z_i), degree of rate control ($X_{RC,i}$), and surface coverage (θ_{j^*}). We note that the onset potential for FePc-catalyzed ORR (E = 1.0 V vs RHE) is well-below the O_2/H_2O equilibrium potential (E = 1.23 V vs RHE); therefore, ORR is far from equilibrium throughout the studied potential range and $\vec{\alpha}_{ORR} = \alpha_{ORR}$.

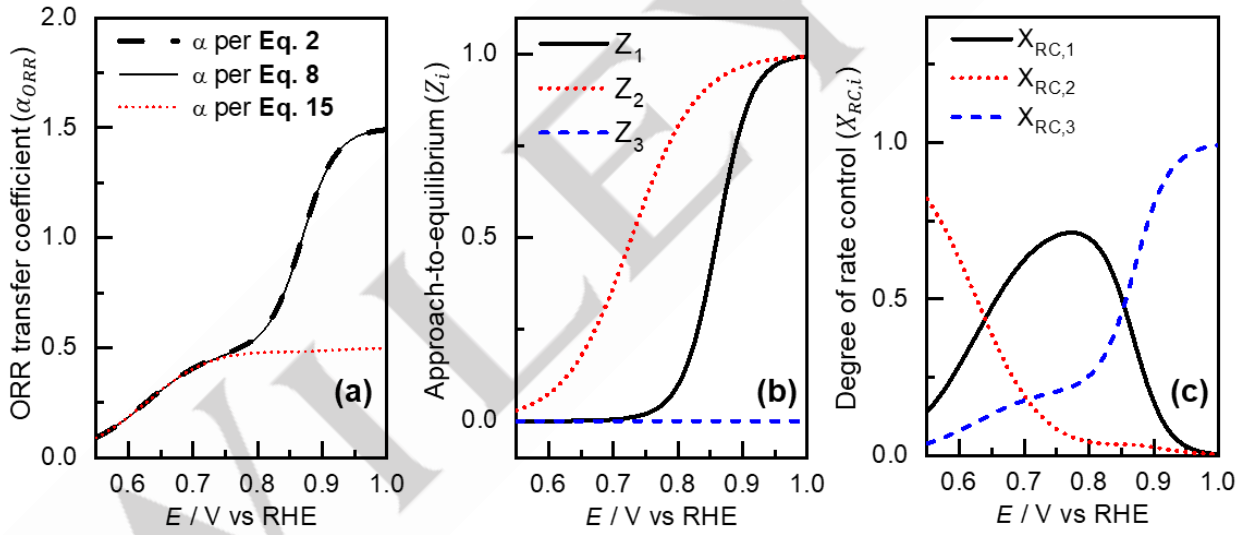

Figure 7. Steady-state kinetic descriptors of the oxygen reduction reaction (ORR) calculated by numerical integration of the microkinetic model per the mechanism and regressed parameters reported in

Table 2. **(a)** ORR transfer coefficient (α_{ORR}) calculated by numerical differentiation (**Eq. 2**, **– –**), the general equation for α derived in this work (**Eq. 8**, —), and the specific form of **Eq. 8** in the case of total faradaic irreversibility (**Eq. 15**, •••). **(b)** Approach-to-equilibrium and **(c)** degree of rate control of step 1 (**—**), step 2 (•••), and step 3 (– –).

Figure 7(a) shows α_{ORR} calculated by direct numerical differentiation (– – –) varies from ~1½ to < 0.1 as overpotential is increased (or E is decreased). Near the onset potential (E = 1.0 V vs RHE), $\alpha_{ORR} \approx$ 1½ is well-described by **Eq. 3** in correspondence with rate-determining formation of OOH* (step 3) preceded by pre-equilibrium faradaic OH* desorption (step 1) and non-faradaic O_2 adsorption (step 2) as shown in **Figure 6**. For $E \lesssim$ 0.9 V vs RHE, α_{ORR} decreases without plateau to a second cardinal regime observed in examples hereinabove. Instead, α_{ORR} decreases continuously and appears to tend to zero as overpotential increases. Throughout these

potential-driven evolutions in α_{ORR}, **Eq. 8** (—) agrees quantitatively with **Eq. 2**—suggesting that the mechanistic origin of non-cardinal, E-dependent transfer coefficient is manifest in Z_i and $X_{RC,i}$. To this end, we examine $Z_{i=1-3}$ and $X_{RC,i=1-3}$ respectively reported in **Figure 7(b)** and **Figure 7(c)**. Steps 4–5 are observed to be kinetically-irrelevant for E = 0.55–1.0 V vs RHE and therefore descriptors for these steps are not shown (see Section S11 for details). **Figure 7(b-c)** confirms that near the onset potential (1.0 V vs RHE), **(b)** steps 1 and 2 are pre-equilibrated (Z_1, Z_2 = 1) and **(c)** step 3 is rate-determining ($X_{RC,3}$ = 1). Section S12 also confirms that OH* is the catalyst resting state (θ_{OH^*} = 1). For E < 0.9 V vs RHE, the PEA begins to breakdown as steps 1 and 2 de-equilibrate—evidenced by Z_1, Z_2 < 1 in **Figure 7(b)**. The de-equilibration of steps 1 and 2 exactly coincides with decrease in α_{ORR}, consistent with precepts of **Eq. 8**. From 0.9 V to 0.7 V vs RHE, electrochemical OH* desorption (step 1) is neither equilibrated ($Z_1 = 1$) nor irreversible ($Z_1 \ll 1$). In this potential regime, step 3 is no longer solely rate-determining ($X_{RC,3}$ < 1). Rather, rate control is shared, predominantly amongst steps 1 and 3, which are each non-equilibrated, kinetically-relevant faradaic steps. As a result, from 0.9 V to 0.7 V vs RHE, α_{ORR} cannot be described by **Eq. 3** and instead requires explicit consideration of potential-dependent Z_{1-3} through **Eq. 8**.

For E < 0.7 V vs RHE, OH* electrosorption completely de-equilibrates ($Z_1 \ll 1$; **Figure 7(b)**) and ORR enters the regime of total *faradaic* irreversibility—meaning all *electrochemical* steps are irreversible. Unlike preceding examples, this condition does not specify $\alpha \approx ½$ because of the presence of a kinetically-relevant *chemical* step. **Figure 7(c)** shows that non-faradaic O_2 adsorption exerts increasing rate control as E is decreased below 0.7 V vs RHE. Consequently, the simplified form of **Eq. 8** in the regime of total faradaic irreversibility is not **Eq. 11** but instead

$$\alpha_{ORR} = \sum_{i=1-3} X_{RC,i} n_i \left(\beta_i + \frac{Z_i}{1 - Z_i}\right) \underset{n_2 = 0}{\overset{Z_1, Z_3 \ll 1}{\Longrightarrow}} \frac{1 - X_{RC,2}}{2} \qquad \textbf{(15)}$$

Eq. 15 is shown to accurately describe α_{ORR} for E < 0.7 V vs RHE in **Figure 7(a)** and reveals that, in the regime of total faradaic irreversibility, α_{ORR}—nominally an *electrochemical* descriptor—precisely quantifies the degree of rate control of a *chemical* step, O_2 adsorption. This counterintuitive relationship is a direct consequence of the de-equilibration of faradaic elementary steps and reinforces the mechanistic learnings proffered through generalization of **Eq. 3** to **Eq. 8**.

We surmise that potential-dependent kinetic phenomena such as those predicted by **Eq. 15** can be captured experimentally through measurement and examination of Tafel slope plots (e.g., **Figure 7(a)**) recently showcased as enabling mechanistic tools for study of HER, OER, and CO_2 reduction in acidic and alkaline environments[14,28]. In these examples, E-dependent α are typically regarded as kinetically uninterpretable because of their evident incompatibility with **Eq. 3**. The framework developed in this work offers new opportunities for interpretation of E-dependent α through simple mathematical results such as **Eq. 15** which relate changes in α to a specific molecular event (e.g., O_2 adsorption). We anticipate that the presently unknown mechanistic origins of non-cardinal E-dependent α observed for many electrocatalytic reactions (e.g., HER on Pt(pc) in 0.1 M NaOH[28]) may be clarified by explicit treatment of Z_i (**Eq. 8**)— plausibly in concert with the increasingly recognized importance of thermodynamically non-ideal adsorption[60] and adsorbate surface diffusion[61]. We note that each of these complexities, and any other non-idealities (e.g., temperature-dependent symmetry factors discussed in Section S1[42,43]), are readily captured by the framework developed in this work. In addition, **Eq. 8** is not limited to description of electrocatalytic reactions but is general to any reaction sequence comprised of faradaic elementary step events—including corrosion and thermochemical catalytic reactions driven by local short circuit (LSC), or mixed-potential-driven, mechanisms.

3.3 Case Study III: Aerobic oxidation on supported Pt catalysts

Recent mechanistic studies have demonstrated that thermochemical redox catalysis at metal-liquid interfaces commonly occurs through the coupling of faradaic half-reactions[5,25,30–35]. As an example, oxidative dehydrogenation of formic acid ($HCOOH + ½O_2 \rightarrow CO_2 + H_2O$) at Pt–$H_2O$ interfaces occurs through the coupling of electrochemical formic acid oxidation ($HCOOH \rightarrow CO_2 + 2H^+ + 2e^-$) and O_2 reduction ($½O_2 + 2H^+ + 2e^- \rightarrow H_2O$). The electrochemical potential (E) of the metal catalyst during these LSC reactions is a 'mixed potential' determined by the steady-state passage of electrons (and protons) between each half-reaction, analogously to corrosion mechanisms. The 'mixed potential' (E) of Pt-based catalysts span a broad potential range (0.2 – 0.8 V vs RHE) during aqueous aerobic oxidation reactions based on substrate identity and reaction conditions. Cyclic voltammetry and surface-sensitive spectroscopies indicate that H_2O-solvated Pt surfaces in this potential window vary from hydrogen-covered (0.2 – 0.3 V vs RHE) to bare (0.3 – 0.6 V vs RHE) to oxygen-covered/passivated (> 0.6 V vs RHE)[62]. Irrespective of these distinct surface structures, Pt catalysts competently transfer O atoms to a broad range

of substrates (**Figure 8**). Crucially, the mixed potential of Pt-based catalysts during all these aerobic oxidation reactions are ≥0.2 V negative of O_2 reduction onset (~1 V vs RHE)—indicating that the oxygen reduction pathway is in the totally irreversible regime, much like the case of ORR on FePc discussed above. Therefore, the framework developed hereinbefore informs kinetic and mechanistic study of O_2 activation in each of these reactions. In order to demonstrate the relevance of this work, we compile and analyze electrochemical measurements for mixed-potential-driven aerobic oxidation reactions on supported nanoparticulate Pt—a commonly-used class of heterogeneous catalysts.

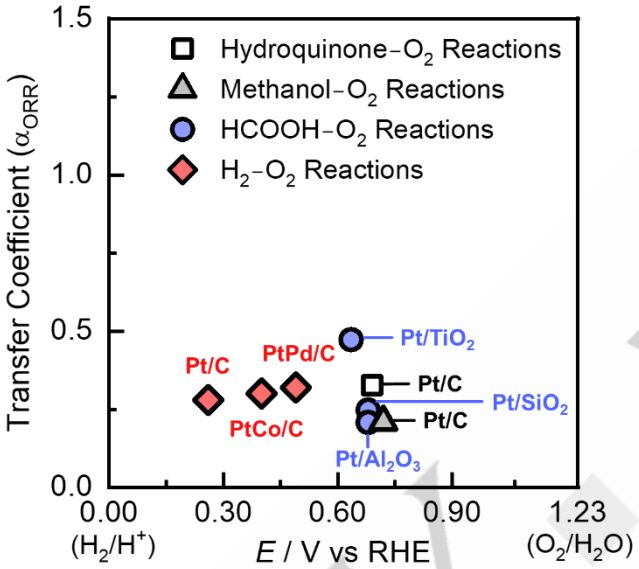

Figure 8. Oxygen reduction reaction (ORR) transfer coefficients (α_{ORR}) measured during thermochemical aqueous aerobic oxidation reactions on Pt-based catalysts[5,63–65]. The potential axis ranges from H_2/H^+ equilibrium (0 V vs RHE) to O_2/H_2O equilibrium (1.23 V vs RHE). RHE refers to the reversible hydrogen electrode. Transfer coefficients are either reproduced from original reports or are determined by digitization and regression of reported polarization curves. Data are labeled with the corresponding catalyst performing aerobic oxidation reactions with substrates indicated in legend. Details regarding data analysis and description of reaction conditions are provided in Section S13.

The x-axis of **Figure 8** reports steady-state mixed potentials measured for a range of aqueous aerobic oxidation reactions on monometallic Pt and Pt alloy catalysts. The co-reaction of HCOOH and O_2 on supported Pt catalysts in 0.1 M $HClO_4$ (○ in **Figure 8**), for example, leads to E ~ 0.6 V vs RHE. Crucially, this corresponds to a ~0.4 V overpotential relative to the onset potentials for HCOOH oxidation (~0.2 V vs RHE) and O_2 reduction (~1.0 V vs RHE)[65]. As a result, both electrochemical half-reactions likely operate in the regime of total faradaic irreversibility much like the CER (E > 0.2 V vs Cl_2/Cl^-) and ORR (E < 0.7 V vs RHE) case studies above. The mathematical and conceptual tools developed in this work (e.g., **Eqs. 8, 11, 15**) are therefore ideally suited to guide mechanistic interpretation of α for each coupled half-reaction—a key descriptor of LSC mechanisms. As a means of demonstration, we compare steady-state α_{ORR} during aerobic oxidation reactions at Pt-H_2O interfaces on the y-axis of **Figure 8**. ORR transfer coefficients (α_{ORR}) in LSC reactions are measured by either (i) linear sweep voltammetry about the steady-state mixed potential or (ii) systematic variation of reductant/substrate concentration which implicitly varies E with identical kinetic consequence as conventional voltammetric protocols. **Figure 8** shows that (i) steady-state mixed potentials are < 0.75 V vs RHE and therefore in the regime of total faradaic irreversibility for the ORR half-reaction and (ii) α_{ORR} are ≤ ½ in agreement with **Eqs. 11** and **15** which respectively described the total irreversibility regime for the CER and ORR case studies above. Indeed, for many of the examples in **Figure 8**, α_{ORR} is significantly below ½ similarly to the case of ORR on Fe-Pc catalysts. The consistency of $\alpha_{ORR} \lesssim ½$ across metal, support, and substrate identity indicates that, under the far-from-equilibrium conditions of LSC mechanisms, ORR plausibly occurs through mechanisms with shared rate-control between electrochemical steps and chemical steps (e.g., $O_2 + * \rightarrow O_2*$ akin to Fe-Pc catalysts). Based on these analysis, we advise that mechanistic proposals of LSC reactions consider the propensity for non-equilibrium mixed potentials to cause (i) every electrochemical elementary step to become irreversible and (ii) a condition-dependent competition between kinetically-relevant faradaic and non-faradaic elementary steps—as has recently been proposed for glucose–O_2 reactions[66] and non-oxidative formic acid dehydrogenation[24] on Pt-group metal surfaces. Moreover, we highlight that comparison of E and α_{ORR} across a suite of alloys (Pt/C, PtCo/C, PtPd/C; ◆ in **Figure 8**) or differently-supported monometallic catalysts (Pt/SiO_2, Pt/Al_2O_3, Pt/TiO_2; ○ in **Figure 8**) provides new opportunities to formulate

structure–function relationships. Complementary to established periodic trends in *standard state* adsorption energies, the framework outlined herein enables comparative interpretation of *operando*, non-equilibrium energetic descriptors (E) and their influence on kinetic observables (α_{ORR}). Comparison of differently supported Pt catalysts (○ in **Figure 8**), for example, reveals that while Pt/SiO_2 and Pt/Al_2O_3 display $\alpha_{ORR} \approx 0.2$, Pt/TiO_2 displays $\alpha_{ORR} \approx 0.5$ in the same potential range (E = 0.64 – 0.68 V vs RHE) during HCOOH–O_2 reactions. These observations indicate that ORR on Pt/TiO_2 occurs via a series of irreversible electrochemical steps ($\alpha_{ORR} \approx 0.5$) while ORR on Pt/SiO_2 and Pt/Al_2O_3 proceeds through a combination of kinetically-relevant electrochemical *and* chemical steps ($\alpha_{ORR} <$ 0.5). Similarly, comparison of differently alloyed C–supported Pt catalysts (◇ in **Figure 8**) reveals that alloying Pt with Co and Pd leads to systematic changes in the catalyst potential (E = 0.40 – 0.56 V vs RHE) without any appreciable change in the ORR transfer coefficient (α_{ORR} = 0.28 – 0.32)—suggesting that, under conditions of H_2–O_2 catalysis, the ORR pathway is totally irreversible on each Pt alloy and kinetically insensitive to alloy-induced changes to E = 0.40 – 0.56 V vs RHE. The developments in this work enable mechanistic interpretation such as these not only during mixed-potential-driven aerobic oxidations but in any multi-step charge transfer process.

4. Conclusion

In this Scientific Perspective, we present a general expression for the Tafel slope (or transfer coefficient) of multi-step charge transfer reactions in terms of the degree of rate control and approach-to-equilibrium of each constituent elementary step. This equation generalizes the ubiquitously used 'cardinal' Tafel slope formula to account for (i) any distribution of rate-determining steps and resting states and (ii) the (in)accuracy of the pre-equilibrium approximation—a core tenet of the 'cardinal' Tafel slope analysis. By recasting Tafel slope in explicit terms of elementary-step approach-to-equilibrium, we show that multi-step electrochemical reactions are susceptible to a condition of complete irreversibility, wherein every molecular charge-transfer event becomes unidirectional. We explore the onset and kinetic consequences of this condition through examination of several case studies, including the chlorine evolution reaction (CER) on metallic Pt-Ir alloy catalysts and oxygen reduction reaction (ORR) on molecular Fe-phthalocyanine catalysts. From analysis of experimental data available in the literature, we find the CER and ORR reactions become totally irreversible for overpotentials ~150 mV vs Cl_2/Cl^- and ~300 mV vs ORR onset respectively. The condition of total faradaic irreversibility causes a necessary transition in Tafel slope to $\gtrsim$ 120 mV/dec. From surveyal of reported electrokinetic studies for H_2 evolution/oxidation, O_2 evolution/reduction, and CO reduction, we demonstrate that this transition in Tafel slope from cardinal values 30, 40, 60 mV/dec to $\gtrsim$ 120 mV/dec is a common feature of electrocatalytic reactions generally explainable by a breakdown in the pre-equilibrium approximation and establishment of total irreversibility. At these conditions, Tafel slope provides *no information* regarding the identity of rate-determining electrochemical elementary steps. Instead, information of rate-determining step identity is manifest in surface coverages (i.e., catalyst resting state identity), thus motivating development and application of methods to enumerate populations of reaction intermediates under catalytic conditions. These conclusions are extended to thermochemical catalytic reactions mediated by corrosion mechanisms—an expansive class of chemistries monikered local-short circuit reactions (LSC). Meta-analysis of LSC aerobic oxidation reactions on Pt-based catalysts reveals a similar preponderance of Tafel slope $\gtrsim$ 120 mV/dec, which indicates that thermochemical redox reactions tend to induce non-equilibrium conditions for which faradaic elementary steps must be irreversible. Together, these case studies demonstrate the broad utility of the conceptual and mathematical framework outlined in this Scientific Perspective to inform mechanistic interpretation of multi-step charge transfer reactions in terms of kinetics and thermodynamics of each elementary step.

Supporting Information

Supporting information contains mathematical derivations, additional calculations, and details regarding analysis of available literature data. Sample code for calculation of kinetic descriptors and simulation of microkinetic models will be provided upon reasonable request.

Acknowledgements

This work was supported by the Director, Office of Science, Office of Basic Energy Sciences, Chemical Sciences, Geosciences, and Biosciences Division, of the U.S. Department of Energy under Contract DE-AC02-05CH11231, FWP CH030201 (Catalysis Research Program).

Keywords: Tafel slope • transfer coefficient • pre-equilibrium • degree of rate control • reversibility

References:

1. Jin, Q. & Bethke, C. M. Kinetics of electron transfer through the respiratory chain. *Biophys. J.* **83**, 1797–1808 (2002).

2. Chen, D. *et al.* Mechanistic Insights into Oxygen Exchange in Mixed Ionic-Electronic Conductors: A Current–Voltage Study. *Chem. Mater.* **36**, 11635–11644 (2024).

3. Lee, S. *et al.* Elucidating the Pivotal Role of Acid-Catalyzed Hydration in Electrochemical Carbon Corrosion. *ACS Catal.* **14**, 17293–17302 (2024).

4. Shinagawa, T., Garcia-Esparza, A. T. & Takanabe, K. Insight on Tafel slopes from a microkinetic analysis of aqueous electrocatalysis for energy conversion. *Sci. Rep.* **5**, (2015).

5. Adams, J. S., Kromer, M. L., Rodríguez-López, J. & Flaherty, D. W. Unifying Concepts in Electro- And Thermocatalysis toward Hydrogen Peroxide Production. *J. Am. Chem. Soc.* **143**, 7940–7957 (2021).

6. Shin, S. & Metiu, H. Nonadiabatic effects on the charge transfer rate constant: A numerical study of a simple model system. *J. Chem. Phys.* **102**, 9285–9295 (1995).

7. Hush, N. S. Adiabatic Rate Processes at Electrodes. I. Energy-Charge Relationships. *J. Chem. Phys.* **28**, 962–972 (1958).

8. Hammes-Schiffer, S. Proton-Coupled Electron Transfer: Moving Together and Charging Forward. *J. Am. Chem. Soc.* **137**, 8860–8871 (2015).

9. Zhang, Y. *et al.* Lithium-ion intercalation by coupled ion-electron transfer. *Science (80-.).* **390**, eadq2541 (2025).

10. Fletcher, S. Tafel slopes from first principles. *J. Solid State Electrochem.* **13**, 537–549 (2009).

11. Bockris, J. O. & Nagy, Z. Symmetry Factor and Transfer Coefficient A source of confusion in electrode kinetics. *J. Chem. Educ.* **50**, 839–843 (1973).

12. Horiuti, J. & Ikusima, M. Mechanism of the Hydrogen Electrode Process on Platinum. *Proc. Imp. Acad.* **15**, 39–44 (1939).

13. Bediako, D. K., Surendranath, Y. & Nocera, D. G. Mechanistic Studies of the Oxygen Evolution Reaction Mediated by a Nickel–Borate Thin Film Electrocatalyst. *J. Am. Chem. Soc.* **135**, 3662–3674 (2013).

14. van der Heijden, O., Vos, R. E. & Koper, M. T. M. Temperature-Dependent Kinetic Parameters for the Alkaline Oxygen Evolution Reaction on NiFeOOH. *ACS Energy Lett.* **10**, 3040–3049 (2025).

15. Lim, T. *et al.* General Efficacy of Atomically Dispersed Pt Catalysts for the Chlorine Evolution Reaction: Potential-Dependent Switching of the Kinetics and Mechanism. *ACS Catal.* **11**, 12232–12246 (2021).

16. Ha, H. *et al.* Highly Selective Active Chlorine Generation Electrocatalyzed by Co3O4 Nanoparticles: Mechanistic Investigation through in Situ Electrokinetic and Spectroscopic Analyses. *J. Phys. Chem. Lett.* **10**, 1226–1233 (2019).

17. Schreier, M., Yoon, Y., Jackson, M. N. & Surendranath, Y. Competition between H and CO for Active Sites Governs Copper-Mediated Electrosynthesis of Hydrocarbon Fuels. *Angew. Chemie* **130**, 10378–10382 (2018).

18. Zeng, J. S., Corbin, N., Williams, K. & Manthiram, K. Kinetic Analysis on the Role of Bicarbonate in

Carbon Dioxide Electroreduction at Immobilized Cobalt Phthalocyanine. *ACS Catal.* **10**, 4326–4336 (2020).

19. Chu, A. T. & Surendranath, Y. Aprotic Solvent Exposes an Altered Mechanism for Copper-Catalyzed Ethylene Electrosynthesis. *J. Am. Chem. Soc.* **144**, 5359–5365 (2022).

20. Jin, K. *et al.* Epoxidation of Cyclooctene Using Water as the Oxygen Atom Source at Manganese Oxide Electrocatalysts. *J. Am. Chem. Soc.* **141**, 6413–6418 (2019).

21. Chung, M. *et al.* Direct propylene epoxidation via water activation over Pd-Pt electrocatalysts. *Science (80-.).* **383**, 49–55 (2024).

22. Bondue, C. J. & Koper, M. T. M. A mechanistic investigation on the electrocatalytic reduction of aliphatic ketones at platinum. *J. Catal.* **369**, 302–311 (2019).

23. Chung, M., Jin, K., Zeng, J. S. & Manthiram, K. Mechanism of Chlorine-Mediated Electrochemical Ethylene Oxidation in Saline Water. *ACS Catal.* **10**, 14015–14023 (2020).

24. Qi, X. *et al.* Potential–Rate Correlations of Supported Palladium-Based Catalysts for Aqueous Formic Acid Dehydrogenation. *J. Am. Chem. Soc.* **146**, 9191–9204 (2024).

25. Wang, H.-X. & Surendranath, Y. Thermochemical heterolytic hydrogenation catalysis proceeds through polarization-driven hydride transfer. *Nat. Chem.* **18**, 43–50 (2025).

26. Westendorff, K. S., Hülsey, M. J., Wesley, T. S., Román-Leshkov, Y. & Surendranath, Y. Electrically driven proton transfer promotes Brønsted acid catalysis by orders of magnitude. *Science (80-.).* **383**, 757–763 (2024).

27. Marshall, A. T. & Vaisson-Béthune, L. Avoid the quasi-equilibrium assumption when evaluating the electrocatalytic oxygen evolution reaction mechanism by Tafel slope analysis. *Electrochem. commun.* **61**, 23–26 (2015).

28. van der Heijden, O., Park, S., Vos, R. E., Eggebeen, J. J. J. & Koper, M. T. M. Tafel Slope Plot as a Tool to Analyze Electrocatalytic Reactions. *ACS Energy Lett.* **9**, 1871–1879 (2024).

29. Khadke, P. *et al.* A simple and effective method for the accurate extraction of kinetic parameters using differential Tafel plots. *Sci. Rep.* **11**, 8974 (2021).

30. Kim, B. *et al.* Tafel Analysis Predicts Cooperative Redox Enhancement Effects in Thermocatalytic Alcohol Dehydrogenation. *ACS Catal.* **14**, 8488–8493 (2024).

31. Harraz, D. M., Lodaya, K. M., Tang, B. Y. & Surendranath, Y. Homogeneous-heterogeneous bifunctionality in Pd-catalyzed vinyl acetate synthesis. *Science (80-.).* **388**, eads7913 (2025).

32. An, H., Sun, G., Hülsey, M. J., Sautet, P. & Yan, N. Demonstrating the Electron–Proton-Transfer Mechanism of Aqueous Phase 4-Nitrophenol Hydrogenation Using Unbiased Electrochemical Cells. *ACS Catal.* **12**, 15021–15027 (2022).

33. Daniel, I. T. *et al.* Electrochemical Polarization of Disparate Catalytic Sites Drives Thermochemical Rate Enhancement. *ACS Catal.* **13**, 14189–14198 (2023).

34. Yan, M., Namari, N. A. P., Nakamura, J. & Takeyasu, K. Theoretical framework for mixed-potential-driven catalysis. *Commun. Chem.* **7**, 69 (2024).

35. Yan, M., Asif, M., Singh, R., Takeyasu, K. & Nakamura, J. Mixed-Potential-Driven Catalysis: An Electrochemical Mechanism for Room-Temperature CO Oxidation on Gold Catalysts. *Adv. Sci.* **12**, e05994 (2025).

36. Foley, B. L. & Bhan, A. Degree of rate control and De Donder relations-An interpretation based on

transition state theory. *J. Catal.* **384**, 231–251 (2020).

37. Campbell, C. T. The Degree of Rate Control: A Powerful Tool for Catalysis Research. *ACS Catal.* **7**, 2770–2779 (2017).

38. Baz, A. & Holewinski, A. Predicting macro-kinetic observables in electrocatalysis using the generalized degree of rate control. *J. Catal.* **397**, 233–244 (2021).

39. Razdan, N. K., Lin, T. C. & Bhan, A. Concepts Relevant for the Kinetic Analysis of Reversible Reaction Systems. *Chem. Rev.* **123**, 2950–3006 (2023).

40. Dumesic, J. A. Analyses of Reaction Schemes Using De Donder Relations. *J. Catal.* **185**, 496–505 (1999).

41. Foley, B. L. & Bhan, A. Thermodynamically consistent forward and reverse degrees of rate control in reversible reactions. *J. Catal.* **389**, 566–577 (2020).

42. Noh, S., Cho, Y. J., Zhang, G. & Schreier, M. Insight into the Role of Entropy in Promoting Electrochemical CO2 Reduction by Imidazolium Cations. *J. Am. Chem. Soc.* **145**, 27657–27663 (2023).

43. Conway, B. E., Tessier, D. F. & Wilkinson, D. P. Experimental evidence for the potential-dependence of entropy of activation in electrochemical reactions in relations to the temperature-dependence of tafel slopes. *J. Electroanal. Chem. Interfacial Electrochem.* **199**, 249–269 (1986).

44. Baz, A., Dix, S. T., Holewinski, A. & Linic, S. Microkinetic modeling in electrocatalysis: Applications, limitations, and recommendations for reliable mechanistic insights. *J. Catal.* **404**, 864–872 (2021).

45. Zeng, Y., Smith, R. B., Bai, P. & Bazant, M. Z. Simple formula for Marcus–Hush–Chidsey kinetics. *J. Electroanal. Chem.* **735**, 77–83 (2014).

46. Tilak, B. V. Kinetics of Chlorine Evolution—A Comparative Study. *J. Electrochem. Soc.* **126**, 1343 (1979).

47. Abild-Pedersen, F. Computational catalyst screening: Scaling, bond-order and catalysis. *Catal. Today* **272**, 6–13 (2016).

48. Wang, B. & Zhang, F. Main Descriptors To Correlate Structures with the Performances of Electrocatalysts. *Angew. Chemie Int. Ed.* **61**, e202111026 (2022).

49. Singh, N. *et al.* Quantifying Adsorption of Organic Molecules on Platinum in Aqueous Phase by Hydrogen Site Blocking and in Situ X-ray Absorption Spectroscopy. *ACS Catal.* **9**, 6869–6881 (2019).

50. Chung, D. Y., Lee, K.-J. & Sung, Y.-E. Methanol Electro-Oxidation on the Pt Surface: Revisiting the Cyclic Voltammetry Interpretation. *J. Phys. Chem. C* **120**, 9028–9035 (2016).

51. Samjeské, G., Miki, A., Ye, S. & Osawa, M. Mechanistic Study of Electrocatalytic Oxidation of Formic Acid at Platinum in Acidic Solution by Time-Resolved Surface-Enhanced Infrared Absorption Spectroscopy. *J. Phys. Chem. B* **110**, 16559–16566 (2006).

52. Zhan, C. *et al.* Revealing the CO Coverage-Driven C–C Coupling Mechanism for Electrochemical CO2 Reduction on Cu2O Nanocubes via Operando Raman Spectroscopy. *ACS Catal.* **11**, 7694–7701 (2021).

53. Harrington, D. A. & Conway, B. E. Kinetic theory of the open-circuit potential decay method for evaluation of behaviour of adsorbed intermediates: Analysis for the case of the H2 evolution reaction. *J. Electroanal. Chem. Interfacial Electrochem.* **221**, 1–21 (1987).

54. Circelli, A. R. & Clark, E. L. Elucidating the Origins of Electrocatalytic Phenomena Using Steady State Isotopic Transient Kinetic Analysis. *ACS Catal.* (2026) doi:10.1021/acscatal.6c00526.

55. Tilak, B. V & Conway, B. E. Analytical relations between reaction order and tafel slope derivatives for

electrocatalytic reactions involving chemisorbed intermediates. *Electrochim. Acta* **37**, 51–63 (1992).

56. Holewinski, A. & Linic, S. Elementary Mechanisms in Electrocatalysis: Revisiting the ORR Tafel Slope. *J. Electrochem. Soc.* **159**, 864–870 (2012).

57. Hu, J.-M., Zhang, J.-Q. & Cao, C.-N. Oxygen evolution reaction on IrO2-based DSA® type electrodes: kinetics analysis of Tafel lines and EIS. *Int. J. Hydrogen Energy* **29**, 791–797 (2004).

58. Conway, B. E. & Bai, L. H_2 evolution kinetics at high activity Ni-Mo-Cd electrocoated cathodes and its relation to potential dependence of sorption of H*. *Int. J. Hydrogen Energy* **11**, 533–540 (1986).

59. Snitkoff-Sol, R. Z., Rimon, O., Bond, A. M. & Elbaz, L. Direct measurement of the oxygen reduction reaction kinetics on iron phthalocyanine using advanced transient voltammetry. *Nat. Catal.* **7**, 139–147 (2024).

60. Mayer, J. M. Site heterogeneity and broad surface-binding isotherms in modern catalysis: Building intuition beyond the Sabatier principle. *J. Catal.* **439**, 115725 (2024).

61. Varley, J. B., Govindarajan, N. & Ager, J. W. Understanding the Unique Reactivity of Cu for Electrochemical CO2 Reduction with a 3-Site Model. *J. Phys. Chem. Lett.* **16**, 604–610 (2025).

62. Jerkiewicz, G., Vatankhah, G., Lessard, J., Soriaga, M. P. & Park, Y.-S. Surface-oxide growth at platinum electrodes in aqueous H2SO4: Reexamination of its mechanism through combined cyclic-voltammetry, electrochemical quartz-crystal nanobalance, and Auger electron spectroscopy measurements. *Electrochim. Acta* **49**, 1451–1459 (2004).

63. Qi, X., Obata, K., Hung, C.-K. & Takanabe, K. Bridging mixed potential theory and electrochemical promotion of thermal catalysis during hydroquinone-benzoquinone redox reactions. *Nat. Commun.* **16**, 3646 (2025).

64. Razdan, N. K., Westendorff, K. S. & Surendranath, Y. Wireless potentiometry of thermochemical heterogeneous catalysis. *Nat. Catal.* **8**, 315–327 (2025).

65. Ryu, J. *et al.* Thermochemical aerobic oxidation catalysis in water can be analysed as two coupled electrochemical half-reactions. *Nat. Catal.* **4**, 742–752 (2021).

66. Chung, M., Albrecht, K. O., Terrian, J. M., Broomhead, W. T. & Flaherty, D. W. Surface Coverage Analysis Reveals Potential-Determining Heterolytic Reactions during Thermocatalytic Aerobic Glucose Oxidation. *ACS Catal.* **15**, 13015–13029 (2025).

Entry for the Table of Contents

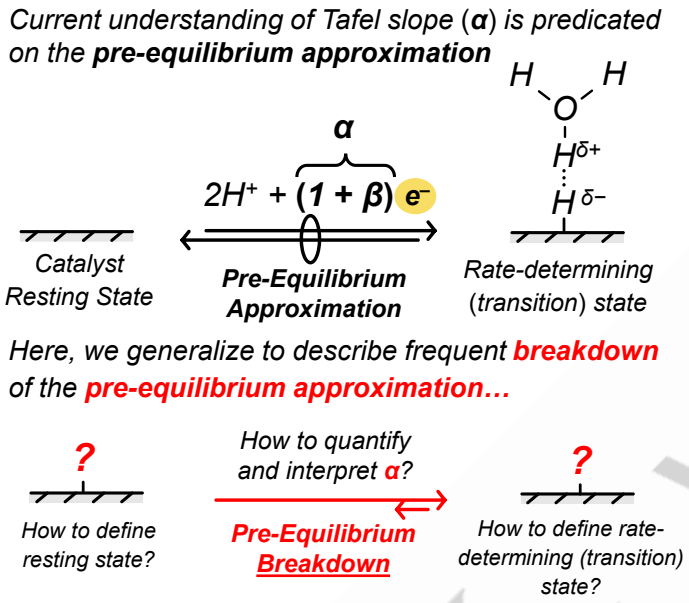

The Tafel slope is a key descriptor of charge transfer kinetics in chemical synthesis, energy conversion, and biological redox. Although Tafel slope is easy to measure, current understanding of the mechanistic meaning of Tafel slope is confined to a narrow set of limiting conditions. Here, we present a universal equation for Tafel slope in exact terms of the kinetics and thermochemistry of elementary steps. This equation redresses key knowledge gaps that have impeded elicitation of molecular information from Tafel slope.